Supporting Information

An Optical Sensing Platform for the Detection of Anti-Cancer Drug and Their Cytotoxicity Screening using A Highly Selective Phosphorene-based Composite

Nasrin Sultana[1,2], Chingtham Thanil Singh[1,2], Mojibur R. Khan[1,2], Neelotpal Sen Sarma[1,2*]

[1]Institute of Advanced Study in Science and Technology, Paschim Boragaon, Guwahati-35, Assam, India

[2]Academy of Scientific and Innovative Research (AcSIR), Ghaziabad-201002, India

***Corresponding author**: neelot@iasst.gov.in

Abbreviation of Supporting Information: **SI**

We have also done the elemental mapping analysis of the synthesized material Ph-Cys-Au for elements like P, Au, S, N, and C, as shown in *figure S1*. We have done the analysis using a field emission-scanning electron microscope (SIGMA VP FESEM, ZEISS).

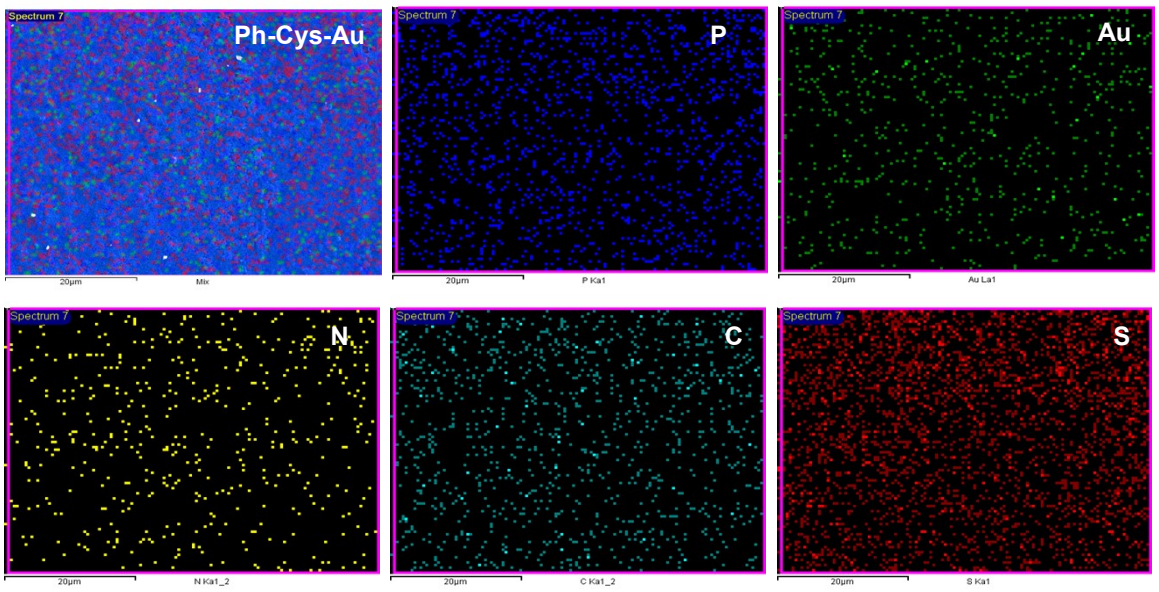

Figure S1: Elemental Mapping of Ph-Cys-Au

We have also characterized the exfoliated Ph using atomic force microscopy (AFM), as shown in *figure S2*. The AFM images have been recorded in the scale 1µm × 1µm and 2µm × 2µm

for different shapes and sizes. The analysis was done by drop-casting the Ph solution on a glass plate. After that, we measured the height profile of the material using the software WSxM 5.0. For the scale 2µm × 2µm and 1µm × 1µm scale, the average thickness was found to be about 60.5 nm and 45 nm, respectively.

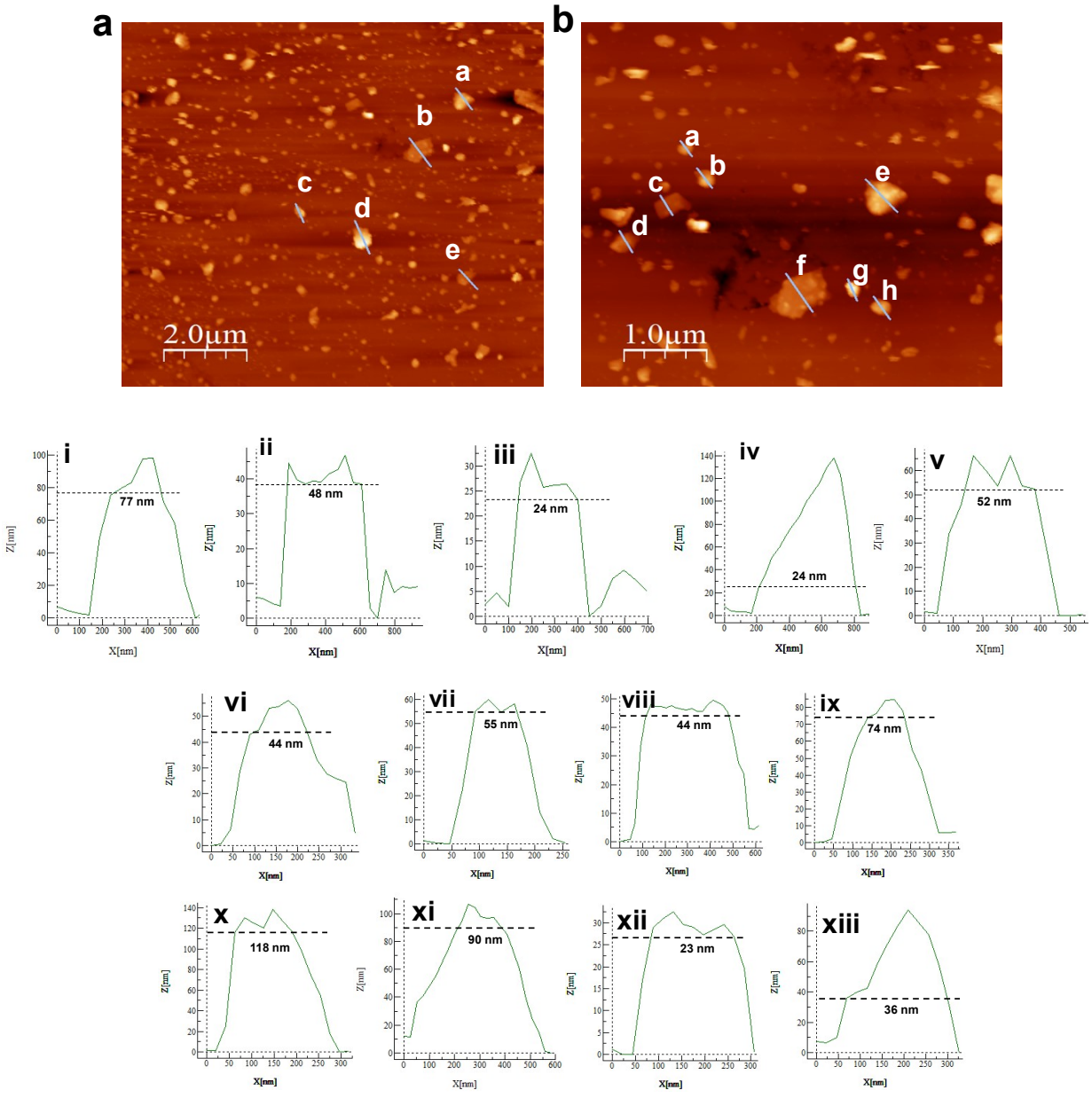

Figure S2: Atomic force microscopy height profile image of few-layer phosphorene sheets produced from ultra-sonication-assisted liquid phase exfoliation of bulk phosphorus in H_2O in the scale (a) 2µm (i-v) and (b)1µm (vi-xii)

As mentioned in the manuscript, we have captured the digital images of the Ph-Cys-Au and Ph-Cys-Au + MTX (before and after sensing) under normal light and UV lamp for aqueous media as shown in *figure S3* below:

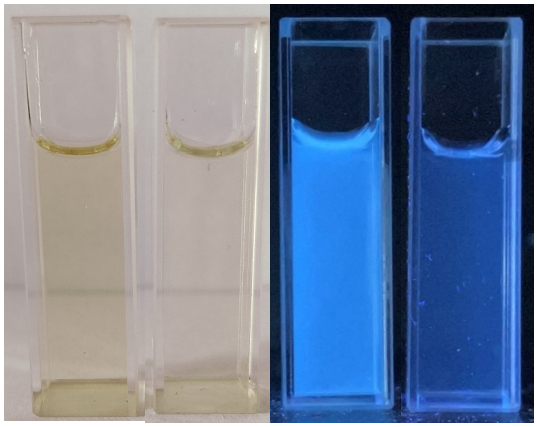

Figure S3: Digital images of the probe and probe + analyte under normal light and UV lamp.

Figure S4 shows the change in intensity at different pH before and after sensing. It has been observed from the graph that, with an increase in the pH, the intensity increases ranging from 1-7. However, no significant change in intensity is observed on further increase of the pH.

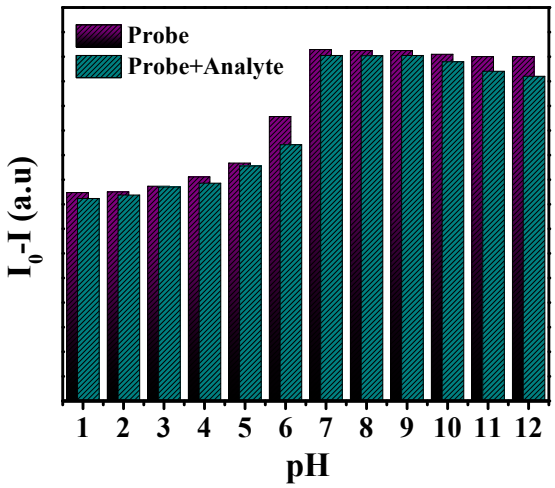

Figure S4: Bar diagram representation of the change in intensity at different pH in the absence and presence of the analyte.

Figure S5 shows the effect of temperature on fluorescent intensity with and without the analyte of choice in the temperature range 15-60 °C. It has been seen from *figure S5 (a)* that with an increase in the temperature, the intensity decreases. We have also plotted the calibration graph for the change in intensity with an increase in the temperature, as shown in *figure S5 (b)*.

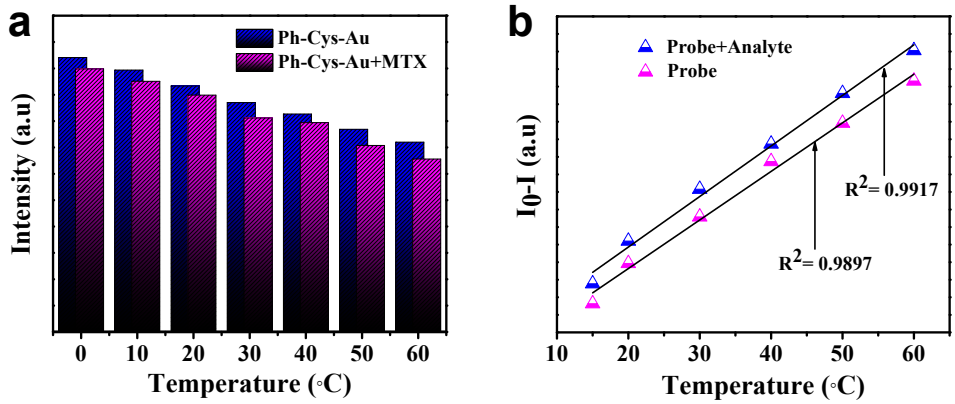

Figure S5: (a) Bar diagram representation of the change in intensity at different temperatures in the absence and presence of the analyte & (b) Calibration graph for the change in intensity with an increase in the temperature.

To check the type of quenching, we have analyzed the UV visible spectra of the probe (Ph-Cys-Au) with an increase in the concentration of the analyte, i.e., MTX, as shown in *figure S6*. At lower concentrations, it does not show any new peak. However, with an increase in the concentration of the analyte, there is a formation of a new peak. This means that the probe shows a dynamic quenching at lower concentrations, and with an increase in the concentration, it starts to form a complex with the analyte. This result can be correlated to the graph obtained from the Stern-Volmer equation, where at lower concentrations, they follow a linear trend. However, with an increase in the concentration of the analyte, the graph becomes concave, indicating the static quenching [1].

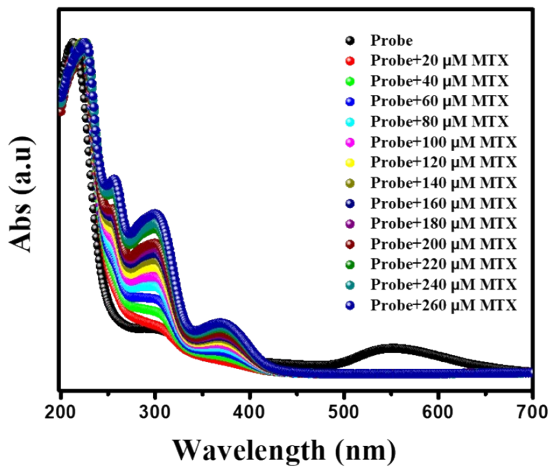

Figure S6: UV visible spectra of Ph-Cys-Au with increase in the concentration of MTX

We have also analyzed the time-resolved photoluminescence (TRPL) spectra to gather more information regarding dynamic and static quenching. *Figure S7* shows the TRPL spectra of the fluorophore in the presence and absence of the analyte of choice. It has been observed from the study that the photoluminescence lifetime decreases in the presence of the analyte, which indicates dynamic quenching. This means that there is a transfer of electrons from the fluorophore donor to the acceptor. We have also calculated the $\chi 2$ value for both systems. For the fluorophore, the lifetime was about 2.4 ns, whereas, in the presence of the analyte, the lifetime was found to be about 1.9 ns which favours the dynamic quenching [2].

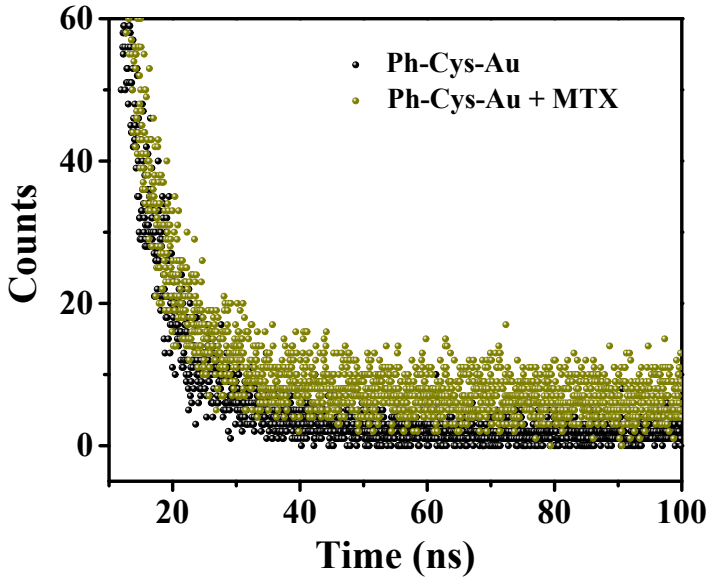

Figure S7: TRPL studies of Ph-Cys-Au and Ph-Cys-Au + MTX

The FRET mechanism is the main driving force responsible for quenching, which can be correlated with the TRPL analysis as there is a change in the lifetime in the presence of the analyte. In the case of FRET, the light emitted by the donor is accepted by the acceptor, which leads to fluorescence quenching. Further, this can be confirmed with the help of the overlap of the absorption spectra of the quencher and the emission spectra of the fluorophore, as shown in *figure S8*. From this figure, we have also calculated the overlap area using the following equation-

$$\text{Overlapping Area} = (\text{Area 1} + \text{Area 2} - \text{Area 3})/ 2$$

Where Area 1 is the area of the emission spectra of the probe, Area 2 is the area of the absorbed spectra of the analyte, and Area 3 is the overall area occupied by both the emission spectra of the probe and the absorbed spectra of the analyte.

The overlapping area was found to be about 33.293, which confirms the transfer of energy from the probe to the analyte.

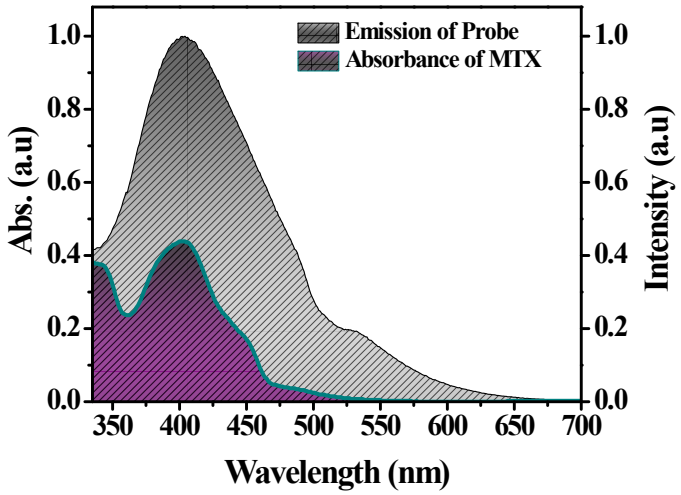

Figure S8: Overlap comparison of absorbance of analyte molecule with the emission spectra of the probe

Figure S9 shows the zeta potential distribution graph for the phosphorene (Ph), Ph-Cys-Au, and Ph-Cys-Au + MTX. They all show negative zeta potential values, i.e., -27.2 eV, -25.3 eV, and -18.3 eV for Ph, Ph-Cys-Au, and Ph-Cys-Au + MTX, respectively. The interaction between the probe and the analyte leads to a significant change in the zeta potential value. This decrease in the zeta potential value implies the electrostatic interaction between the two. This also supports the fact that there may be an aggregation of particles taking place in the system [3].

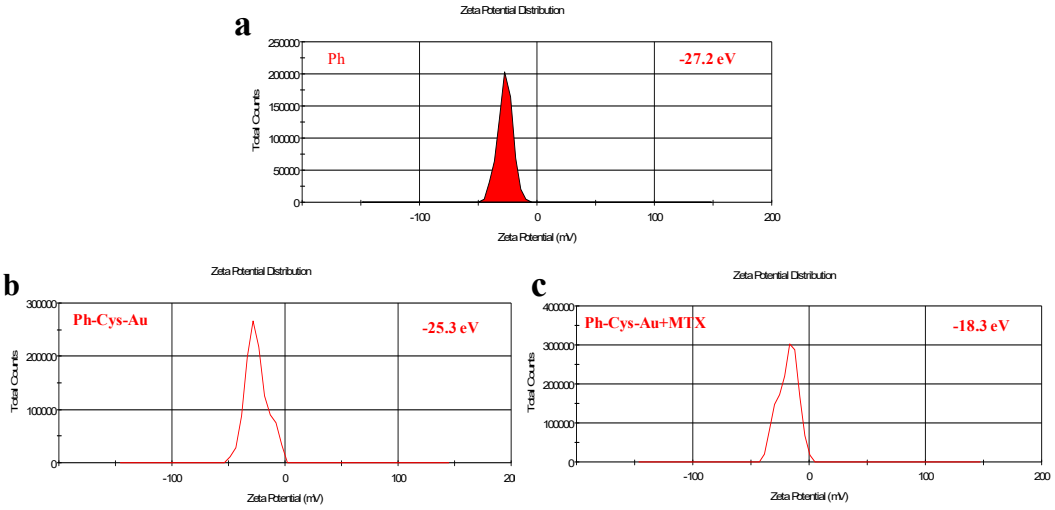

Figure S9: Zeta potential value of (a) Ph; (b) Ph-Cys-Au; and (c) Ph-Cys-Au + MTX

The peaks in the material remained unchanged after coming in contact with the analyte, as shown in the FTIR Spectra (*figure S10)*. However, some of them show a slight change in their characteristic peaks because of the presence of electron-withdrawing groups in the analyte, which may lead to the formation of H-bonding. Apart from these peaks, two of them show a significant change, which is listed below in Table S1. This may be because of the interaction between the P-OH and $–COO^-$ groups present in the probe and the $–NH_2$ group present in the analyte [4]. The change in frequencies observed before and after quenching is listed in table S1.

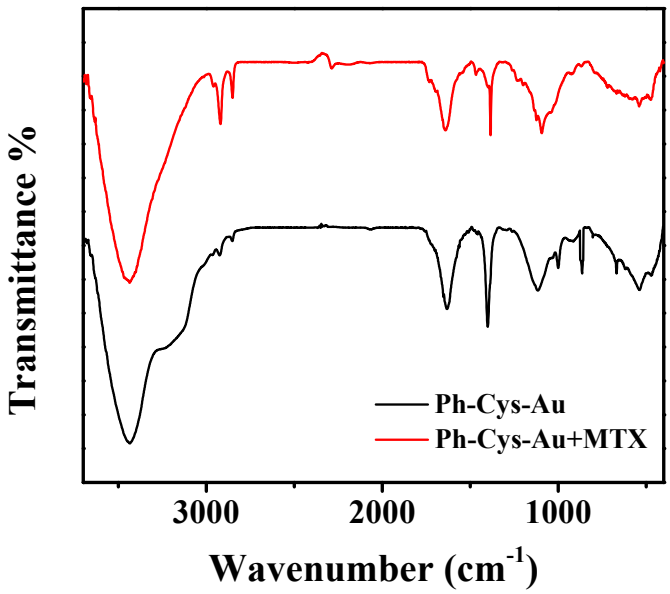

Figure S10: FTIR spectra of Ph-Cys-Au and Ph-Cys-Au + MTX

Table S1: Comparative stretching frequencies of the probe before and after sensing.

Materials	**Frequencies (cm^{-1})**									
Ph-Cys-Au	3437	2924	2854	1634	***1401***	***1119***	998	864	668	536
Ph-Cys-Au + MTX	3437	2921	2952	1638	***1385***	***1094***	998	864	668	541

As shown in *figure S11,* one of the main features of a sensor is that it has to be selective and sensitive enough to detect a particular analyte of choice. It is based on the interaction between the probe and the analyte. Apart from analyzing their quenching efficiency in the case of aqueous media as well as in real samples in the case of MTX, we have also chosen some of the other antibiotics to check their selectivity, as shown in *figure S11 (a)*. For that, we have chosen

analytes like amoxicillin trihydrate (AMOT), azaerythromycin (AZAE), cephalothin sodium salt (CF), cephalexin hydrate (CFL), chloramphenicol (CFP), cefuroxime sodium salt (CFR), colistin sulfate (CLS), cloxacillin sodium (CSX), ivermectin (IVM), nalidixic acid (NA), penicillin sodium salt (PNL), streptomycin sulfate (STM), urasodeoxy cholic acid (UDCS), and vancomycin (VNC) as shown in *figure S11 (b)*. From this analysis, we have found that the quenching efficiency of all these substances is comparatively low compared to MTX.

We have also chosen some other biomolecules, like amino acids and ions, as they are present in the human body and can interfere with sensing. For that purpose, we have analyzed amino acids such as aspartic acid, alanine, glycine, glutamic acid, serine, proline, and ascorbic acid and some ions such as Na^+, K^+, NH^+, and Cl^- as shown in *figure S11 (c)*. From both the bar diagram, it has been observed that the material is highly selective for MTX.

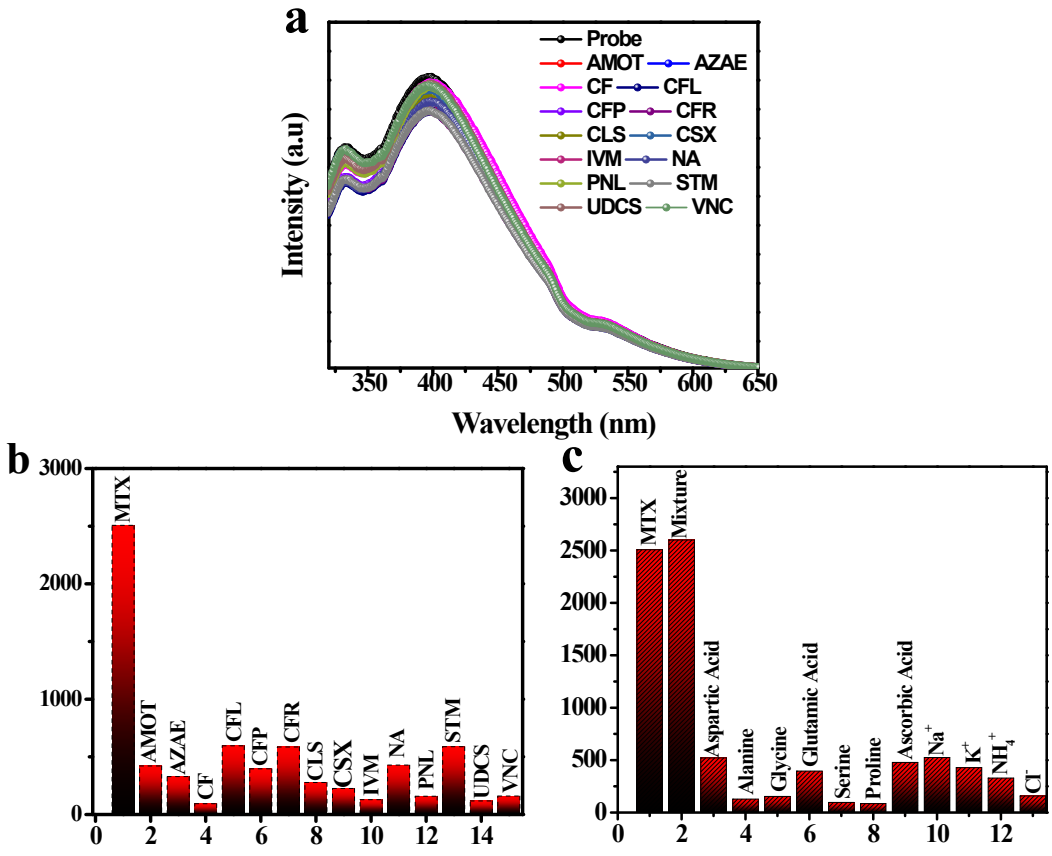

Figure S11: (a) Interference study of other molecules compared to MTX and (b) Interference study of amino acids and ions

References:

1. Goswami, K. J., Sultana, N., & Sarma, N. S., Duel phase selective inner filter effect-based luminescent sensing for the detection of para-nitrophenol and picric acid. Sensors and Actuators B: Chemical, 2023, 374, 132778.
2. Hazarika, I., Goswami, K. J., Hussain, A. A., Kalita, T., Sarma, N. S., & Gogoi, B., Silk fibroin protein as dual mode picric acid sensor and UV photoactive material. Journal of Materials Science, 2021, 56, 18959-18975.
3. Dutta, P., Saikia, D., Adhikary, N. C., & Sarma, N. S., Macromolecular systems with MSA-Capped CdTe and CdTe/ZnS Core/Shell quantum dots as superselective and ultrasensitive optical sensors for picric acid explosive. ACS Applied Materials & Interfaces, 2015, 7(44), 24778-24790.
4. Chakravarty, S., Bhardwaj, N., Mandal, B. B., & Sarma, N. S., Silk fibroin–carbon nanoparticle composite scaffolds: a cost effective supramolecular 'turn off'chemiresistor for nitroaromatic explosive vapours. Journal of Materials Chemistry C, 2016, 4(38), 8920-8929.